

# Effect of Biopolymers on Structure of Hydroxyapatite and Interfacial Interactions in Biomimetically Synthesized Hydroxyapatite/Biopolymer Nanocomposites

DEVENDRA VERMA, KALPANA S. KATTI, and DINESH R. KATTI

Department of Civil Engineering, North Dakota State University, Fargo, ND 58105, USA

(Received 30 July 2007; accepted 4 March 2008; published online 14 March 2008)

**Abstract**—The interfacial interaction and effect of biopolymer on crystal structure of hydroxyapatite in biomimetically synthesized nanocomposites, chitosan/hydroxyapatite (ChiHAP50), polygalacturonic acid/hydroxyapatite (PgAHAP50), and chitosan/polygalacturonic acid/hydroxyapatite (ChiPgAHAP50) have been investigated using atomic force microscopy (AFM), Fourier transform infrared (FTIR) spectroscopy, and Rietveld analysis. AFM phase images show nano-sized hydroxyapatite particles uniformly distributed in biopolymer. FTIR spectra indicate that chitosan interacts with hydroxyapatite through  $\text{NH}_3^+$  groups, whereas in polygalacturonic acid/hydroxyapatite, dissociated carboxylate groups ( $\text{COO}^-$ ) form unidentate chelate with calcium atoms. A change in lattice parameters of hydroxyapatite in all nanocomposites is observed using Rietveld analysis. The increase in lattice parameters was most prominent along c-axis in ChiHAP50 and ChiPgAHAP50 nanocomposites, which was 0.388% and 0.319%, respectively. Comparison between particle sizes of hydroxyapatite, determined from AFM and Rietveld analysis, indicates presence of amorphous phase in hydroxyapatite particles, which is believed to be present at the interface of hydroxyapatite and biopolymer.

**Keywords**—Hydroxyapatite, Chitosan, Polygalacturonic acid, Nanocomposites.

## INTRODUCTION

The “bottoms-up” approach adapted by organisms to produce well-defined hierarchical structure has attracted a great deal of attention.<sup>1,3,15,16,30,39</sup> Organisms produce complex structures containing minerals with controlled size, shape, crystal orientation, polymorphic structure, defect texture, and particle assembly. This process of mineralization in organisms is called as biomineralization. Biomineralization is a complex process, which is controlled by organisms by secretion of various organics, mainly proteins. It is

indeed a challenging task to fully mimic this complex cellular process; however, the material chemistry aspects of biomineralization are being studied to develop materials with desired properties.<sup>10,24,31,36</sup> In this methodology, an organic phase provides a template for inorganic crystals to nucleate and grow from supersaturated solution. Such methodology has shown lot of potential for synthesis of materials with tailor-made properties.<sup>9,11,19,32,38</sup> Organic phase may cause acceleration or inhibition of crystal growth depending on its functionality, molecular weight, concentration, density of functional groups on the backbone chain or side chain, and whether polymer is adsorbed on surface or present in solution.<sup>33</sup> The role of polymers on mineralization has been the focus of many studies.<sup>2,6,17,20,34</sup> Various polymers, both of biological and synthetic origin, with different functionalities have been used to understand fundamental principles governing biomineralization. Amino acids and polymers containing carboxylate groups are specifically found to inhibit growth rate of hydroxyapatite when present in solution.<sup>25</sup> These functional groups have high affinity to bind to calcium ions on growth surface or in solution.

In our previous work, we synthesized composites of chitosan and polygalacturonic acid with hydroxyapatite following a similar approach.<sup>37</sup> The composites were synthesized by allowing precipitation of hydroxyapatite in presence of biopolymers. These nanocomposites were developed for their possible application as bone biomaterials. Three kinds of hydroxyapatite/biopolymer composites were made: chitosan/hydroxyapatite (ChiHAP50), polygalacturonic acid/hydroxyapatite (PgAHAP50), and chitosan/polygalacturonic acid/hydroxyapatite (ChiPgAHAP50). Both chitosan and polygalacturonic acid are biocompatible and biodegradable polysaccharides. Chitosan is one of the most extensively investigated polymers for tissue engineering.<sup>7,8</sup> It promotes cell adhesion, proliferation, and differentiation, and

Address correspondence to Kalpana S. Katti, Department of Civil Engineering, North Dakota State University, Fargo, ND 58105, USA. Electronic mail: kalpana.katti@ndsu.edu

evokes minimal foreign body reaction on implantation. Polygalacturonic acid is a de-esterified pectin. Pectin has been investigated for drug delivery applications.<sup>5,21</sup> Recently, it has also been investigated for possible application in bone tissue engineering.<sup>18</sup> It showed improvement in growth of osteoblast cells. The reason to use these two biopolymers together is to improve the mechanical response of the composites. The major interactions between chitosan and polygalacturonic acid complex are the electrostatic interactions. Polygalacturonic acid being the de-esterified pectin contains higher number of carboxylate groups and is so expected to improve the interfacial interactions and thus mechanical response of the composite. In our previous work the mechanical response of ChiHAP50, PgAHAP50, and ChiPgAHAP50 was conducted and ChiPgAHAP50 showed significant improvement in mechanical properties over ChiHAP50 and PgAHAP50. The particle size, shape, and interfacial interactions in a biomaterial have significant impact on its mechanical response, biocompatibility, and biodegradability. In the current work, we have investigated the effect of biopolymers on crystallite structure, crystal size, and interfacial interactions using atomic force microscopy (AFM), X-ray diffraction (XRD), and Fourier transform infrared (FTIR) spectroscopy.

## MATERIALS AND METHODS

### Materials

$\text{Na}_2\text{HPO}_4$ , ultrapure bioreagent, was obtained from J.T. Baker.  $\text{CaCl}_2$ , GR grade, was obtained from EM Science. Chitosan (deacetylation, >75%) and polygalacturonic acid were obtained from Sigma-Aldrich chemicals. All these chemicals and polymers are used as obtained.

### Hydroxyapatite and Hydroxyapatite/Biopolymer Composites Preparation

The nanocomposites were synthesized using a biomimetic method. The details of synthesis method have been given elsewhere.<sup>37</sup> Briefly, ChiHAP50 and PgAHAP50 are synthesized by dissolving of 2 g of each chitosan and PgA in 1 L of 11.9 mM  $\text{Na}_2\text{HPO}_4$  solution separately. Later, to each of these solutions 1 L of 19.9 mM  $\text{CaCl}_2$  solution was added and further pH was maintained at 7.4 by adding NaOH solution. The precipitates were allowed to settle for 24 h. Further, water was removed by centrifuging followed by drying at 50 °C. ChiPgAHAP50 was synthesized by mixing together  $\text{Na}_2\text{HPO}_4$  solutions containing chitosan and PgA in 1:1 ratio. Further, precipitates were removed by

centrifuging and drying at 50 °C. All these steps except drying were conducted at room temperature.

### Experimental

X-ray powder diffraction studies of hydroxyapatite and hydroxyapatite/biopolymer composites were carried out using a Philips diffractometer using  $\text{CuK}_\alpha$  radiation ( $\lambda = 1.5405 \text{ \AA}$ ). PA-FTIR spectroscopy study was done using Thermo Nicolet, Nexus 870 spectrometer equipped with MTEC Model 300 photoacoustic accessory. Linear photoacoustic spectra (500 scans) of all samples were collected in the range of  $4000\text{--}400 \text{ cm}^{-1}$  at a mirror velocity of 0.15 cm/s. AFM-phase imaging was performed using a Multi-mode<sup>TM</sup> AFM having a Nanoscope-IIIa<sup>TM</sup> controller equipped with a J-type piezo scanner (Veeco Metrology Group, Santa Barbara, CA). Before AFM imaging, all composites were polished under dry conditions using silicon carbide grinding paper (P4000, median particle diameter, 2.5  $\mu\text{m}$ ). The image collection and particle size measurement was performed using NanoScope (R) II software (version—5.30r3.sr3). For each sample, particle sizes of more than 300 particles were performed.

### Structure Refinement

Figures 1–4 show XRD plots of hydroxyapatite, ChiPgAHAP50, ChiHAP50, and PgAHAP50 composites. XRD plots were compared with the joint committee for powder diffraction studies (JCPDS) standard (09-0432). All samples show characteristic peaks of HAP. The major peaks in hydroxyapatite are due to planes (002), (211), (112), (300), (202), (310), (222), (213), and (004). Rietveld analysis of pure

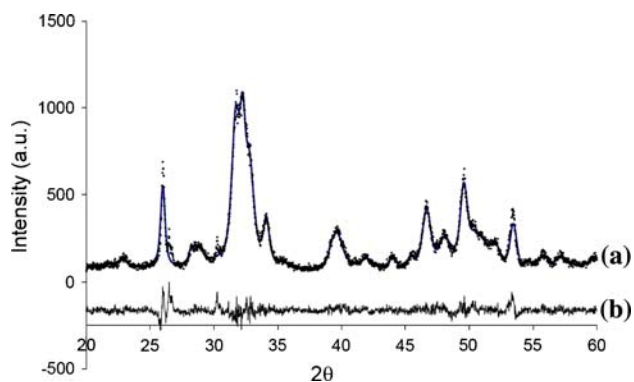


**FIGURE 1.** The experimental XRD plot (a—dots) of hydroxyapatite is superimposed over calculated plot (a—thick solid line). The difference plot (b) of hydroxyapatite is shown at the bottom.

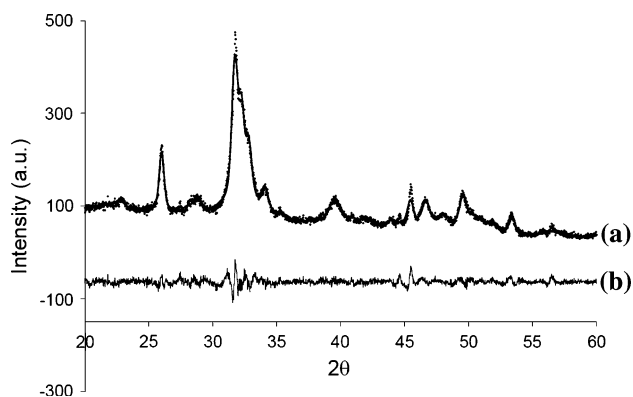


**FIGURE 2.** The experimental XRD plot (a—dots) of PgAHAP50 is superimposed over calculated plot (a—thick solid line). The difference plot (b) of PgAHAP50 is shown at the bottom.

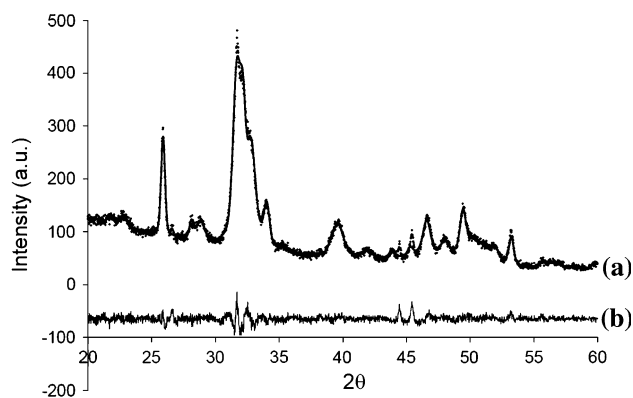


**FIGURE 3.** The experimental XRD plot (a—dotted line) of ChiHAP50 is superimposed over calculated plot (a—thick solid line). The difference plot (b) of ChiHAP50 is shown at the bottom.

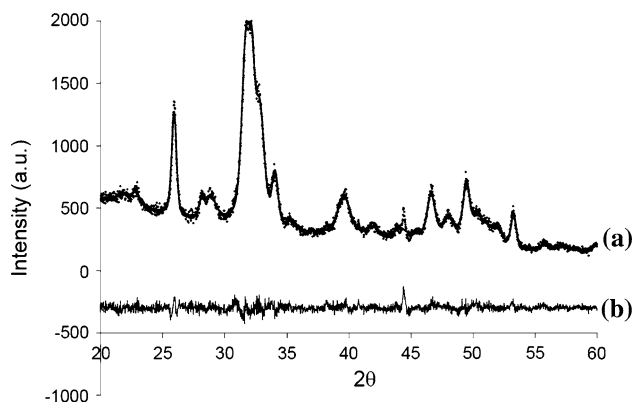


**FIGURE 4.** The experimental XRD plot (a—dotted line) of ChiPecHAP50 is superimposed over calculated plot (a—thick solid line). The difference plot (b) of ChiPecHAP50 is shown at the bottom.

hydroxyapatite and its composites with chitosan, polygalacturonic acid, and both chitosan and polygalacturonic acid were performed using Reflex<sup>TM</sup> module of Materials Studio<sup>TM</sup> (Accelrys Software Inc.) Software. The refinement was done in the range of 20–60° 2 $\theta$ . The lattice parameters of starting model were  $a = b = 9.424 \text{ \AA}$  and  $c = 6.879 \text{ \AA}$  with  $P6_3/m$  space group. The occupancy factor of all atoms was fixed to 1 except for OH. The occupancy factor for OH was fixed at 0.5. The profile function used was Pseudo-Voigt. The temperature factors were refined using atomic anisotropic parameters. The sample parameters: crystallite size, lattice strain, and preferred orientation were also refined. Preferred orientation was refined using March-Dollase function.

## RESULT AND DISCUSSION

### *Nanostructure Analysis Using AFM*

Figures 5a–c show AFM-phase images of PgAHAP50, ChiHAP50, and ChiPgAHAP50 composites. The HAP and biopolymer phases are clearly distinguishable from AFM-phase images. In PgAHAP50, ChiHAP50, and ChiPgAHAP50, the average HAP particle sizes are  $29.9 \pm 8.2 \text{ nm}$ ,  $43.3 \pm 14.9 \text{ nm}$ , and  $32.4 \pm 10.4 \text{ nm}$ , respectively. There are clearly no particularly significant changes in particle sizes observed.

### *Interfacial Interactions*

Figure 6 shows PA-FTIR spectra of HAP, PgA, and PgAHAP50. The band observed at  $1743 \text{ cm}^{-1}$  in PgA is assigned to carbonyl stretching of un-dissociated carboxylate groups. The intensity of this band is significantly reduced in PgAHAP50 as compared to PgA. A new band at  $1615 \text{ cm}^{-1}$  is observed in PgAHAP50. This band is attributed to asymmetric stretching of dissociated carboxylate groups.<sup>14</sup> The presence of band due to dissociated carboxylate groups suggest that in PgAHAP50, PgA interact with hydroxyapatite through dissociated carboxylate groups. Since carboxylate groups are negatively charged, Ca atoms of HAP act as potential sites for attachments. The band at  $2933 \text{ cm}^{-1}$  is assigned to C–H stretching vibration and bands at  $1331$  and  $1234 \text{ cm}^{-1}$  are assigned to C–H bending vibrations of the ring. The band at  $2575 \text{ cm}^{-1}$ , observed as shoulder to the broad OH band at around  $3360 \text{ cm}^{-1}$  originates from OH stretching vibration in free carboxyls bonded by hydrogen bonds into dimers. The absence of this band in PgAHAP50 composite suggests breaking of PgA dimers. The breaking of dimers is consistent with

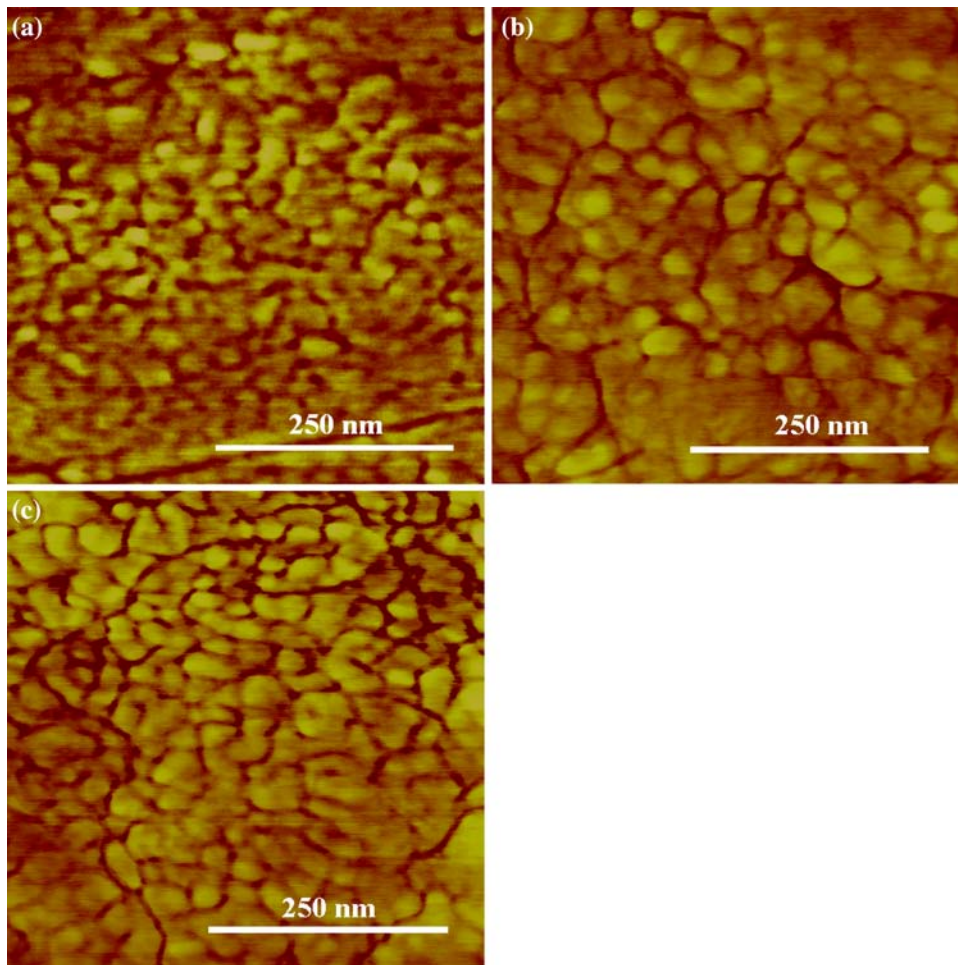


FIGURE 5. AFM-phase image of (a) PgAHAP50 composite, (b) ChiHAP50 composite, and (c) ChiPgAHAP50 composite.

the observation of dissociation of carboxylate groups. The band at  $1422\text{ cm}^{-1}$  in PgAHAP50 composite (Fig. 6) originates from symmetric stretching of carbonyl from dissociated carboxylate groups. The chelation between dissociated groups can be determined from difference in wavenumber between carbonyl asymmetric stretching and symmetric stretching.<sup>13,22</sup> Here, a difference of  $193\text{ cm}^{-1}$  suggests unidentate chelation.

Figure 7 shows PA-FTIR spectra of HAP, chitosan, and ChiHAP50. The bands at  $1653\text{ cm}^{-1}$  and  $1319\text{ cm}^{-1}$  in chitosan are characteristic of *N*-acetylated chitin and are assigned to amide I and amide II bands. The band at  $1593\text{ cm}^{-1}$  in chitosan is assigned to amino characteristic peak.<sup>26</sup> Figure 7 shows chitosan and ChiHPAP50 composites spectra in the range of  $1800\text{--}1200\text{ cm}^{-1}$ . The spectra are normalized with respect to band at  $1376\text{ cm}^{-1}$ . This band originates from C–H symmetric deformation. The second derivative plots (Fig. 8) suggest presence of new bands at around  $1654$ ,  $1558$ , and  $1512\text{ cm}^{-1}$ . Presence of these bands in ChiHAP50 indi-

cates that  $\text{–NH}_2$  transforms to  $\text{–NH}_3^+$ . The bands at  $1654\text{ cm}^{-1}$  and  $1580\text{ cm}^{-1}$  have been assigned to asymmetric deformation and band at  $1512\text{ cm}^{-1}$  is assigned to symmetric deformations of  $\text{–NH}_3^+$ . The presence of  $\text{NH}_3^+$  in ChiHAP50 is consistent with the presence of a band appearing as shoulder to the broad OH band at around  $3340\text{ cm}^{-1}$ . This band is assigned to stretching vibration of  $\text{NH}_3^+$ . The band at around  $2066\text{ cm}^{-1}$  is also characteristic of  $\text{NH}_3^+$  moieties. The  $\text{NH}_3^+$  functional groups being positively charged, forms complex with phosphate ions. This complex further facilitates nucleation and growth of hydroxyapatite.

Figure 9 shows spectra of PgAHAP50, ChiHAP50, and ChiPgAHAP50. To have a better insight into interfacial interaction in ChiPgAHAP50 composites, a comparison between the photoacoustic FTIR spectrum of ChiPgAHAP50 and the spectrum obtained by addition of ChiHAP50 and PgAHAP50 spectra with 50% weightage of each has been done (Fig. 10). As seen, the comparison between these spectra suggests that, ChiPgAHAP50 composite does not result from

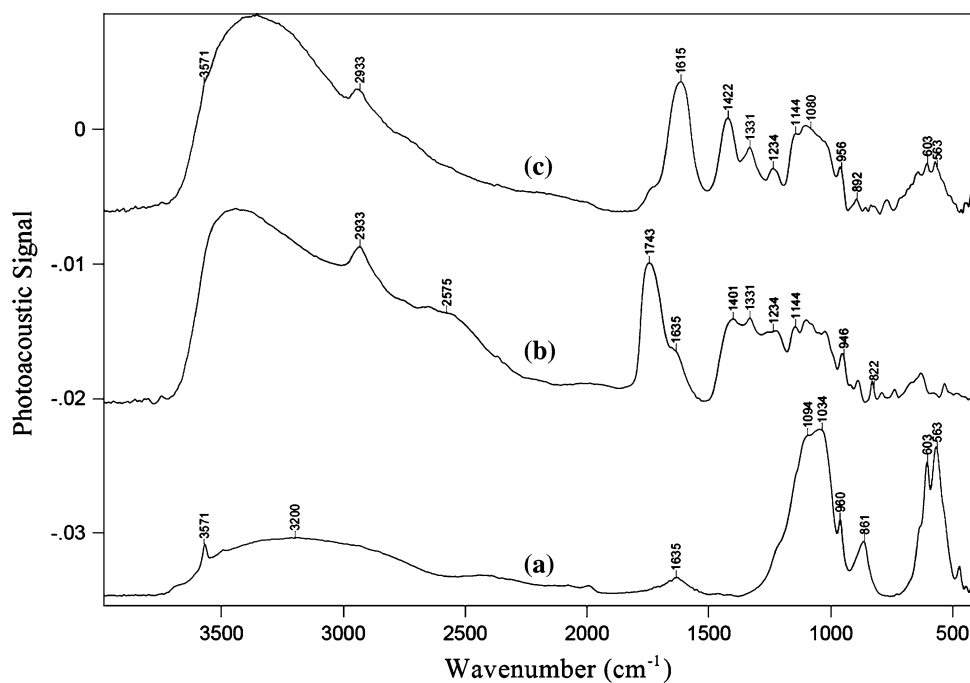


FIGURE 6. Photoacoustic FTIR spectra of (a) hydroxyapatite, (b) PgA, and (c) PgAHAP50 in the region of 4000–400  $\text{cm}^{-1}$  obtained at mirror velocity of 0.15  $\text{cm/s}$ .

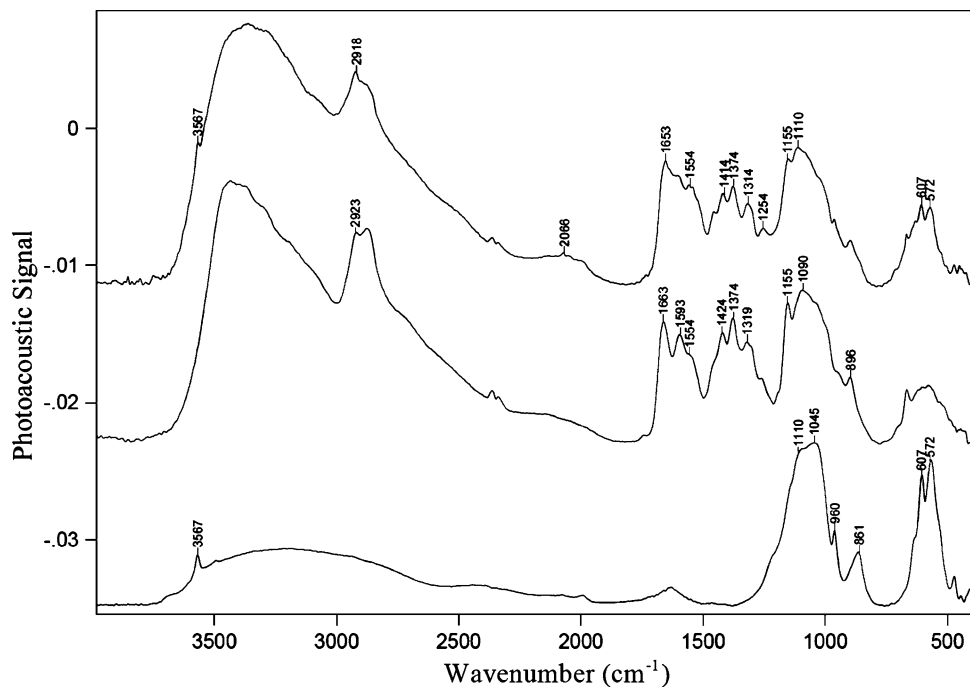
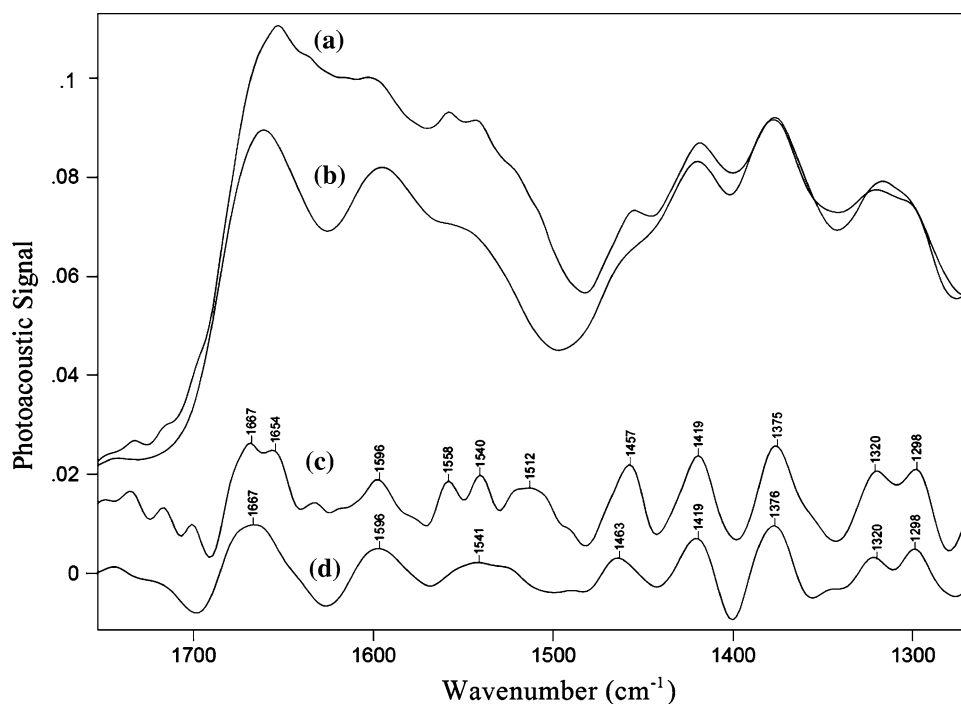


FIGURE 7. Photoacoustic FTIR spectra of (a) hydroxyapatite, (b) chitosan, and (c) ChiHAP50 in the region of 4000–400  $\text{cm}^{-1}$  obtained at mirror velocity of 0.15  $\text{cm/s}$ .

simple mixing of ChiHAP50 and PgAHAP50, but there are further interfacial interactions occurring in the composite. The intensity of band at around 1743  $\text{cm}^{-1}$  is lower in ChiPgAHAP50 composites and

also intensity of band at around 1815  $\text{cm}^{-1}$  and 1422  $\text{cm}^{-1}$  is higher compared to mathematically added spectrum. The above-mentioned observations clearly indicate that carboxylate groups further



**FIGURE 8.** Photoacoustic FTIR spectra of (a) ChiHAP50, (b) chitosan, (c) second derivative plot of ChiHAP50 spectrum, and (d) second derivative plot of chitosan spectrum in the region of 1800–1200  $\text{cm}^{-1}$  obtained at mirror velocity of 0.15  $\text{cm/s}$ .

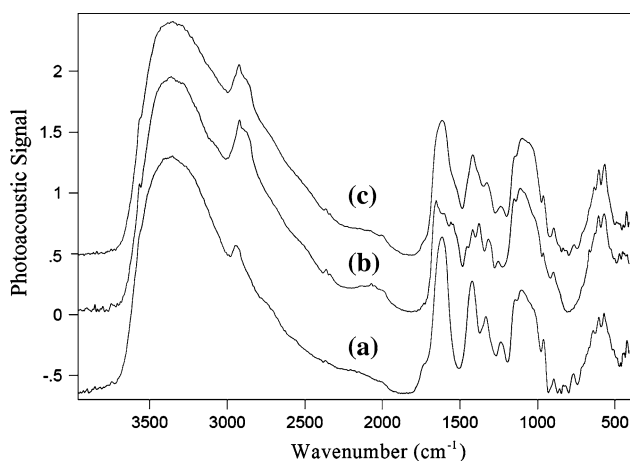


**FIGURE 9.** Photoacoustic FTIR spectra of (a) PgAHAP50, (b) ChiGAP50, and (c) ChiPgAHAP50 in the region of 4000–400  $\text{cm}^{-1}$  obtained at mirror velocity of 0.15  $\text{cm/s}$ .

dissociate and are involved in interfacial interactions between ChiHAP50 and PgAHAP50 particles. These dissociated carboxylate groups may interact with hydroxyapatite phase or chitosan functional groups present on the surface of the ChiHAP50 particles. It is also observed that there are changes in phosphate stretching and bending regions. This suggests that phosphate groups of hydroxyapatite are also involved in the interfacial interactions.

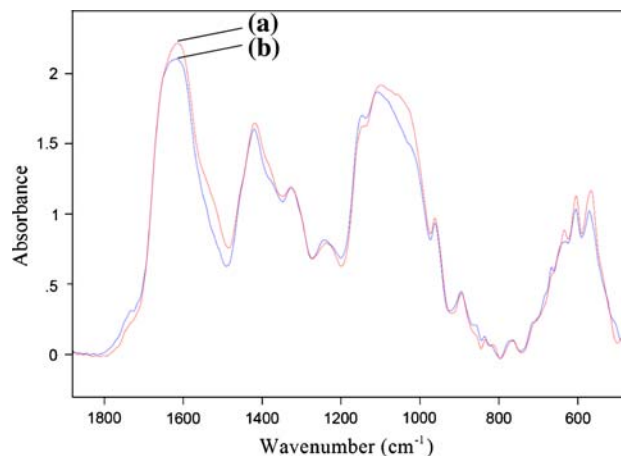


**FIGURE 10.** Photoacoustic FTIR spectra (1800–700  $\text{cm}^{-1}$ ) of (a) ChiPgAHAP50 and (b) mathematically added (PgAHAP50 + ChiHAP50) in the region of 1800–700  $\text{cm}^{-1}$  obtained at mirror velocity of 0.15  $\text{cm/s}$ .

#### *Effect of Biopolymers on Structure of Hydroxyapatite*

Hydroxyapatite crystallizes in a hexagonal crystal lattice with  $P6_3/m$  space group.<sup>12</sup> The lattice parameters calculated from Rietveld refinement are given in Table 1. The Rietveld analysis indicates that there is a change in lattice parameters of hydroxyapatite present in biopolymer/hydroxyapatite nanocomposites as compared to pure hydroxyapatite. The biomimetic hydroxyapatite showed similar trend in all nanocom-

posites, i.e., positive shift (elongation) was observed along c-axis whereas negative shift (contraction) was observed along a-axis ( $a = b$ ). The elongation along c-axis was significantly higher in ChiHAP50 and ChiPgAHAP50 than PgAHAP50 (Table 2). This large change is rather significant in a ceramic material such as HAP. The composites consist of nano-sized HAP particles and hence a very large surface interacts with biopolymers. This large interfacial interaction may lead to large lattice distortions of hydroxyapatite. The shift in ChiHAP50 and ChiPgAHAP50 was significantly higher than PgAHAP50 composites, which suggest that the shift in lattice parameters also depend on the type of biopolymers. Recently, the change in lattice parameters of biogenic aragonite of nacre (biological composite) has been reported.<sup>27–29</sup> Nacre is an inner iridescent layer of many mollusk seashells and made of aragonite platelets of thickness  $\approx 0.5 \mu\text{m}$  separated by organic layers primarily composed of proteins. The organic content in nacre varies from 2% to 5%. Pokroy *et al.* have shown that shift in lattice parameters of biogenic aragonite is a widespread phenomenon in mollusk seashell species.<sup>27</sup> The shift along c-axis was as high as 0.2% in some species. The origin of lattice distortions in biogenic aragonite has

been attributed to organics present within the aragonite platelets.

Our results indicate that crystal distortions by organics are not limited to mollusk phylum; it can also be achieved by following a biomimetic synthesis method. The spatial mismatch between functional groups of biopolymer and hydroxyapatite lattice sites can cause residual stresses at the biopolymer/mineral interface. This residual stress can lead to distortion in the crystal structure of hydroxyapatite. The second phenomenon, which could cause stress on crystal lattice, is the conformational change in biopolymers, while compaction of composites during drying.

For further understanding of structure of hydroxyapatite nanoparticles, the crystallite sizes of hydroxyapatite determined from Rietveld analysis were compared with their particle sizes determined from AFM images. The crystallite sizes calculated from Rietveld analysis are found to be smaller compared to the particle size determined from AFM-phase images (Table 3). This suggests that either HAP particles observed from AFM-phase images have multi-granular structure or they contain significant amount of amorphous phase. The difference between particle size and their respective crystallite size is more pronounced in ChiHAP50 and ChiPgAHAP50. The growth of hydroxyapatite particles in presence of chitosan or PgA resemble the biomineralization process, where proteins and other biopolymers control the growth of the mineral. Nacre, the protein-aragonite composite is one such example. The presence of amorphous phase at polymer/mineral interface is also being found in nacre.<sup>23</sup>

The functional sites of biopolymers act as a nucleating site for crystallization of mineral. The negatively charged carboxylate groups of polygalacturonic acid are known for their calcium binding ability. The dissociated carboxylate groups and calcium ions form a complex, which initiate further growth of hydroxyapatite.<sup>4,35</sup> On the other hand, in case of chitosan, amine being positively charged, form complex with phosphate groups. Because, these nucleating sites in chitosan or polygalacturonic acid are not spatially arranged and oriented to have perfect match with lattice sites of phosphate or calcium ions, it is most likely that hydroxyapatite precipitate as amorphous phase near polymer surface (Fig. 11). DiMasi *et al.* investigated

**TABLE 1. Lattice parameters determined from Rietveld analysis XRD data.**

	HAP (Å)	ChiHAP50 (Å)	PgAHAP50 (Å)	ChiPgAHAP50 (Å)
<i>a, b</i>	9.464	9.460 ↓	9.453 ↓	9.455 ↓
<i>c</i>	6.856	6.882 ↑	6.858 ↑	6.878 ↑

The (↓) symbol depicts decrease in lattice parameter of biomimetic hydroxyapatite with respect to hydroxyapatite and (↑) symbol depicts increase in lattice parameters of biomimetic hydroxyapatite with respect to pure hydroxyapatite.

**TABLE 2. The percentage change in lattice parameters of biomimetic hydroxyapatite with respect to pure hydroxyapatite.**

	ChiHAP50 (%)	PgAHAP50 (%)	ChiPgAHAP50 (%)
<i>a, b</i>	-0.019	-0.085	-0.068
<i>c</i>	+0.388	+0.039	+0.319

**TABLE 3. Crystallite sizes of biomimetic hydroxyapatite from Rietveld analysis using XRD data.**

	HAP (nm)	ChiHAP50 (nm)		PgAHAP50 (nm)		ChiPgAHAP50 (nm)	
		X-ray	AFM	X-ray	AFM	X-ray	AFM
<i>a, b</i>	11.1	17.2 ± 1.2	43.3 ± 14.9	23.9 ± 2.9	28.9 ± 8.2	10.0 ± 0.3	32.4 ± 10.4
<i>c</i>	17.1	28.5 ± 2.5		16.4 ± 1.0		16.5 ± 0.4	

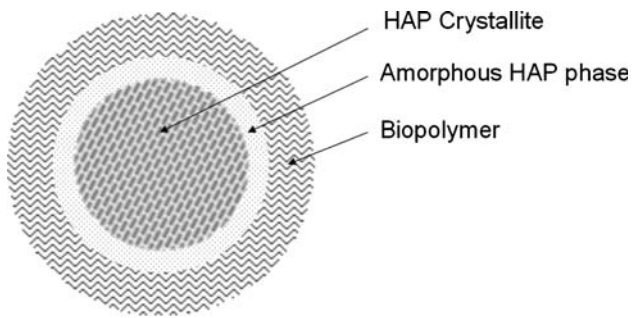


**FIGURE 11.** Schematic showing amorphous phase in PgA-HAP50, ChiHAP50, and ChiPgAHAP50 nanocomposites.

precipitation of mineral from supersaturated calcium carbonate solution on fatty acid monolayer. They observed that precipitation of mineral started with amorphous hydrated calcium carbonate phase.<sup>9</sup>

### CONCLUSIONS

In this work, we have investigated the interfacial molecular interactions between biopolymers and hydroxyapatite. Also analyzed is the effect of biopolymer on structure of hydroxyapatite in biomimetic composites using Rietveld analysis. The intermolecular interactions between different components have been studied using FTIR spectroscopy. The FTIR spectra indicate that in PgAHAP50, polygalacturonic acid attaches to hydroxyapatite surface through dissociated carboxylate groups, whereas in ChiHAP50, chitosan interacts with hydroxyapatite through NH groups. The FTIR results also indicate that in ChiPgAHAP50 composites, chitosan, PgA, and hydroxyapatite, all participate in interfacial interactions. The AFM-phase images indicate a uniform dispersion of hydroxyapatite nanoparticles in biopolymer matrix. A comparison between hydroxyapatite particle size determined from AFM imaging and Rietveld analysis, suggest either hydroxyapatite particles have multi-granular structure or may contain significant amount of amorphous phase. Rietveld analysis has also shown a change in lattice parameters of biomimetic hydroxyapatite. A significant change in crystal structure may potentially arise from existence of amorphous phase at the interface. The shift in lattice parameters was found to be highest along c-axis in chitosan containing (ChiHAP50 and ChiPgAHAP50) nanocomposites. A change of 0.4% in the structure of hydroxyapatite is observed. This is a rather significant change resulting from nanoscale interaction of biopolymer and mineral. It is expected that such weak interactions also occur in many biological and bio-replacement materials which

result in significant changes to lattice structure of mineral.

### ACKNOWLEDGMENTS

This work is partially supported by a grant from National Science Foundation (CAREER # 0132768). Author D.V. would like to acknowledge support from NDSU Graduate School Doctoral Dissertation award.

### REFERENCES

- <sup>1</sup>Aizenberg, J., A. Tkachenko, S. Weiner, L. Addadi, and G. Hendler. Calcitic microlenses as part of the photoreceptor system in brittlestars. *Nature* 412:819–822, 2001.
- <sup>2</sup>Belcher, A. M., P. K. Hansma, G. D. Stucky, and D. E. Morse. First steps in harnessing the potential of biomineralization as a route to new high-performance composite materials. *Acta Mater.* 46:733–736, 1998.
- <sup>3</sup>Belcher, A. M., X. H. Wu, R. J. Christensen, P. K. Hansma, G. D. Stucky, and D. E. Morse. Control of crystal phase switching and orientation by soluble mollusc-shell proteins. *Nature* 381:56–58, 1996.
- <sup>4</sup>Bhowmik, R., K. S. Katti, D. Verma, and D. R. Katti. Probing molecular interactions in bone biomaterials: through molecular dynamics and Fourier transform infrared spectroscopy. *Mater. Sci. Eng. C* 27:352–371, 2007.
- <sup>5</sup>Chambin, O., G. Dupuis, D. Champion, A. Voilley, and Y. Pourcelot. Colon-specific drug delivery: influence of solution reticulation properties upon pectin beads performance. *Int. J. Pharma.* 321:86–93, 2006.
- <sup>6</sup>Dalas, E., J. K. Kallitsis, and P. G. Koutsoukos. Crystallization of hydroxyapatite on polymers. *Langmuir* 7:1822–1826, 1991.
- <sup>7</sup>Dang, J. M., and K. W. Leong. Natural polymers for gene delivery and tissue engineering. *Adv. Drug Del. Rev.* 58:487–499, 2006.
- <sup>8</sup>Di Martino, A., M. Sittinger, and M. V. Risbud. Chitosan: a versatile biopolymer for orthopaedic tissue-engineering. *Biomaterials* 26:5983–5990, 2005.
- <sup>9</sup>DiMasi, E., V. M. Patel, M. Sivakumar, M. J. Olszta, Y. P. Yang, and L. B. Gower. Polymer-controlled growth rate of an amorphous mineral film nucleated at a fatty acid monolayer. *Langmuir* 18:8902–8909, 2002.
- <sup>10</sup>Duplat, D., M. Puisségur, L. Bédouet, M. Rousseau, H. Boulzaguet, C. Milet, D. Sellos, A. V. Wormhoudt, and E. Lopez. Identification of calconectin, a calcium-binding protein specifically expressed by the mantle of *Pinctada margaritifera*. *FEBS Lett.* 580:2435–2441, 2006.
- <sup>11</sup>Hall, S. R. Biomimetic synthesis of high- $T_c$  type-II superconductor nanowires. *Adv. Mater.* 18:487–490, 2006.
- <sup>12</sup>Haverty, D., S. A. M. Tofail, K. T. Stanton, and J. B. McMonagle. Structure and stability of hydroxyapatite: density functional calculation and Rietveld analysis. *Phys. Rev. B Condens. Matter Mater. Phys.* 71:1–9, 2005.
- <sup>13</sup>Hu, H., J. Saniger, J. G. Alejandro, and V. M. Castano. Fourier transform infrared spectroscopy studies of the



- reaction between polyacrylic acid and metal oxides. *Mater. Lett.* 12:281–285, 1991.
- <sup>14</sup>Kato, K., Y. Eika, and Y. Ikada. In situ hydroxyapatite crystallization for the formation of hydroxyapatite/polymer composites. *J. Mater. Sci.* 32:5533–5543, 1997.
- <sup>15</sup>Katti, K. S., and D. R. Katti. Why is nacre so tough and strong? *Mater. Sci. Eng. C* 26:1229–1456, 2005.
- <sup>16</sup>Katti, K. S., D. R. Katti, S. M. Pradhan, and A. Bhosle. Platelet interlocks are the key to toughness and strength in nacre. *J. Mater. Res.* 20:1097–1100, 2005.
- <sup>17</sup>Katti, K. S., P. Turlapati, D. Verma, R. Bhowmik, P. K. Gujjula, and D. R. Katti. Static and dynamic mechanical behavior of hydroxyapatite-polyacrylic acid composites under simulated body fluid. *Am. J. Biochem. Biotechnol.* 2:73–79, 2006.
- <sup>18</sup>Liu, L., Y. J. Won, P. H. Cooke, D. R. Coffin, M. L. Fishman, K. B. Hicks, and P. X. Ma. Pectin/poly(lactide-co-glycolide) composite matrices for biomedical applications. *Biomaterials* 25:3201–3210, 2004.
- <sup>19</sup>Lu, C., L. Qi, J. Ma, H. Cheng, M. Zhang, and W. Cao. Controlled growth of micropatterned, oriented calcite films on a self-assembled multilayer film. *Langmuir* 20:7378–7380, 2004.
- <sup>20</sup>Mann, S., D. D. Archibald, J. M. Didymus, T. Douglas, B. R. Heywood, F. C. Meldrum, and N. J. Reeves. Crystallization at inorganic-organic interfaces: biomaterials and biomimetic synthesis. *Science* 261:1286–1292, 1993.
- <sup>21</sup>Mundargi, R. C., S. A. Patil, S. A. Agnihotri, and T. M. Aminabhavi. Development of polysaccharide-based colon targeted drug delivery systems for the treatment of amoebiasis. *Drug Dev. Ind. Pharm.* 33:255–264, 2007.
- <sup>22</sup>Nakamoto, K. Infrared and Raman Spectra of Inorganic and Coordination Compounds, Part B. New York: John Wiley & Sons, 1997.
- <sup>23</sup>Nassif, N., N. Pinna, N. Gehrke, M. Antonietti, C. Jäger, and H. Cölfen. Amorphous layer around aragonite platelets in nacre. *Proc. Natl. Acad. Sci.* 102:12653–12655, 2005.
- <sup>24</sup>Nudelman, F., B. A. Gotliv, L. Addadi, and S. Weiner. Mollusk shell formation: mapping the distribution of organic matrix components underlying a single aragonite tablet in nacre. *J. Struct. Biol.* 153:176–187, 2006.
- <sup>25</sup>Oner, M., and O. Dogan. Inhibitory effect of polyelectrolytes on crystallization kinetics of hydroxyapatite. *Prog. Cryst. Growth Character. Mater.* 50:39–51, 2005.
- <sup>26</sup>Pawlak, A., and M. Mucha. Thermogravimetric and FTIR studies of chitosan blends. *Thermochim. Acta* 396:153–166, 2003.
- <sup>27</sup>Pokroy, B., A. N. Fitch, F. Marin, M. Kapon, N. Adir, and E. Zolotoyabko. Anisotropic lattice distortions in biogenic calcite induced by intra-crystalline organic molecules. *J. Struct. Biol.* 155:96–103, 2006.
- <sup>28</sup>Pokroy, B., A. N. Fitch, and E. Zolotoyabko. The microstructure of biogenic calcite: a view by high-resolution synchrotron powder diffraction. *Adv. Mater.* 18:2363–2368, 2006.
- <sup>29</sup>Pokroy, B., J. P. Quintana, E. N. Caspi, A. Berner, and E. Zolotoyabko. Anisotropic lattice distortions in biogenic aragonite. *Nat. Mater.* 3:900–902, 2004.
- <sup>30</sup>Rodríguez-Navarro, A. B., C. CabraldeMelo, N. Batista, N. Morimoto, P. Alvarez-Lloret, M. Ortega-Huertas, V. M. Fuenzalida, J. I. Arias, J. P. Wiff, and J. L. Arias. Microstructure and crystallographic-texture of giant barnacle (*Austromegabalanus psittacus*) shell. *J. Struct. Biol.* 156:355–362, 2006.
- <sup>31</sup>Rousseau, M., E. Lopez, P. Stempfle, M. Brendle, L. Franke, A. Guette, R. Naslain, and X. Bourrat. Multiscale structure of sheet nacre. *Biomaterials* 26:6254–6262, 2005.
- <sup>32</sup>Tlatlik, H., P. Simon, A. Kawska, D. Zahn, and R. Kniep. Biomimetic fluorapatite-gelatin nanocomposites: prestructuring of gelatin matrices by ion impregnation and its effect on form development. *Angew. Chem. Int. Ed.* 45:1905–1910, 2006.
- <sup>33</sup>Tsotos, A., and G. Nancollas. The role of polycarboxylic acids in calcium phosphate mineralization. *J. Colloid Interface Sci.* 250:159–167, 2002.
- <sup>34</sup>Verma, D., K. S. Katti, and D. R. Katti. Bioactivity in in situ hydroxyapatite-polycaprolactone composites. *J. Biomed. Mater. Res.* 78A:772–780, 2006.
- <sup>35</sup>Verma, D., K. S. Katti, and D. R. Katti. Experimental investigation of interfaces in hydroxyapatite/polyacrylic acid/polycaprolactone composites using photoacoustic FTIR spectroscopy. *J. Biomed. Mater. Res. Part A* 77A:59–66, 2006.
- <sup>36</sup>Verma, D., K. S. Katti, and D. R. Katti. Photoacoustic FTIR spectroscopic study of undisturbed nacre from red abalone. *Spectrochem. Acta Part A* 64:1051–1057, 2006.
- <sup>37</sup>Verma, D., K. S. Katti, and D. R. Katti. Mechanical response, multilevel structure of biomimetic hydroxyapatite/polygalacturonic acid/chitosan nanocomposites. *Mater. Sci. Eng. C* 28:399–405, 2008.
- <sup>38</sup>Volkmer, D., M. Harms, L. Gower, and A. Ziegler. Morphosynthesis of nacre-type laminated CaCO<sub>3</sub> thin films and coatings. *Angew. Chem. Int. Ed.* 44:639–644, 2005.
- <sup>39</sup>Weiner, S., and L. Addadi. Design strategies in mineralized biological materials. *J. Mater. Chem.* 7:689–702, 1997.